Sweta Shrestha

30th Hayes Research Forum

Water as Solar Fuel: Development of Zeolite-Supported Manganese Oxides Catalysts

Abstract:

In this work zeolite supported manganese oxides (MnOx-Y) were studied for photochemical water oxidation. Zeolite-supported manganese oxides were synthesized by ion-exchanging of manganese ions into zeolite pores and cages, and pulling out those cations by treating with potassium permanganate and precipitating them manganese oxides on the surface of zeolite. Prepared zeolite-supported manganese oxides were treated with high concentration of potassium ions, which ion-exchanges into zeolite channels as well as manganese oxides. Bulk manganese oxides (MnOx) were also synthesized from manganese salts and permanganate in aqueous medium. Characterizations such as powder x-ray diffraction (PXRD), Raman spectroscopy, x-ray photoelectron spectroscopy (XPS), and electron microscopy provided the information about the structural features of MnOx-Y and those features match to poorly ordered birnessites (layered like manganese oxides). Photochemical water oxidation of MnOx-Y and MnOx were evaluated using $Ru(bpy)_3^{2+}$-$S_2O_8^{2-}$ system. MnOx-Y exhibited better catalytic activity compared to bulk MnOx, showing that zeolite support is the important factor for enhancing the catalytic activity of manganese oxides for photochemical water oxidation. A non-impregnation route provided by zeolite support has offered an advantage for the deposition of manganese oxides on its surface. Zeolite support provides a high surface area scaffold for wide dispersion of manganese oxides on its surface, which brings the catalyst and photosensitizer in a close proximity for efficient electron transfer between them during water oxidation.

Introduction:

Today 82% of world's energy supply are dependent on non-renewable fossil fuels such as coal, oil, and natural gas (1). With the rise of global population and advanced technologies, the demand of global energy supply is increasing at an alarming rate. Burning these fossil fuels is also a primary reason for global warming, which produces massive amount of greenhouse gases such as CO_2 (record breaking level: 400 ppm level) (2). In order to resolve these critical issues, a clean, sustainable, and renewable sources of energy is of urgency. Hydrogen gas (H_2) can be a potential source of clean and renewable energy carrier (3). H_2 gas is used in hydrogen fuel cells, hydrocracking, urea synthesis, and many other areas. Currently about most of the H_2 fuel is generated from burning fossil fuels, and the process involves generating greenhouse gases which is not ideal, environment-friendly or cost-effective. Photocatalytic water splitting could be the clean, sustainable, and economical method to generate H_2 gas (4). This process involves using abundant renewable resources such as water and sunlight as the source of energy. In this process, water decomposes into oxygen (O_2) and H_2 using solar energy. The generated H_2 gas could be stored and consumed as a clean fuel.

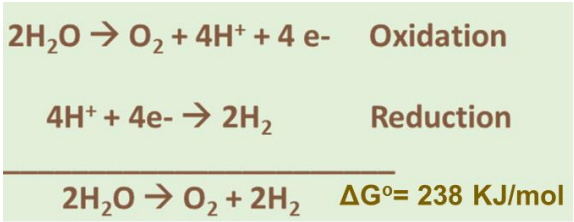

Figure 1: Water-splitting reaction (water oxidation and water reduction)

Water splitting process consists of two steps: water oxidation and water reduction. Water oxidation step involves oxidation of water into O_2 gas, protons, and electrons. And water reduction involves using generated protons and electrons to produce H_2 gas. The water oxidation step is thermodynamically and kinetically unfavorable reaction as it is a multi-electron process. It is an

uphill reactions ($\Delta G = 238$ KJ/mol). Without an efficient water oxidation step, the water splitting process can be quite challenging. Thus this step requires the best O_2 evolving catalyst (water oxidizing catalyst) so that it can drive water oxidation step efficiently and consequently the production of H_2 gas becomes efficient.

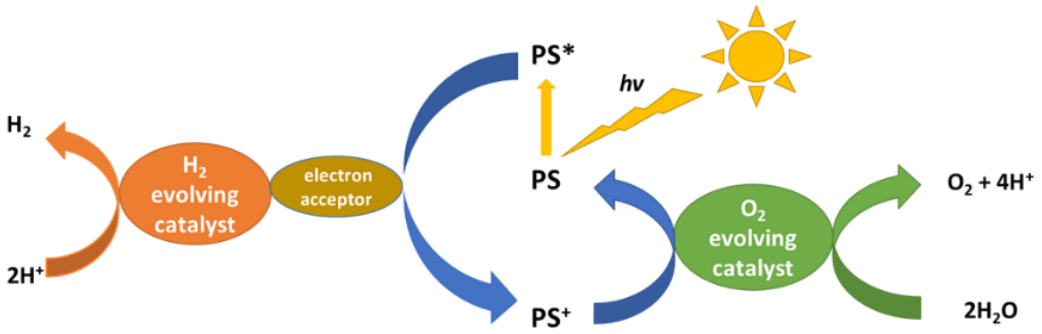

Figure 2: Water-splitting reaction using photosensitizer (PS) to trap sunlight in photochemical system

Several homogeneous and heterogeneous catalysts have been explored for water oxidation study. Heterogeneous oxides such as oxides of iridium oxide (5) and ruthenium oxide (6) have been reported to be efficient water oxidizing catalysts, but they are impractical as they are rare expensive metals. Earth abundant transition metals such as iron, cobalt, nickel, oxides have been studied as water oxidizing catalysts (7-9). Metal oxides supported and un-supported on several matrices have been reported as well.

Manganese oxides have been reported to be efficient water oxidizing catalysts. Manganese is abundant, non-toxic, and economical element. It is also found in enzyme responsible for water oxidation in natural photosynthesis. Different polymorphs of manganese oxides such as α-Mn_2O_3, α-MnO_2, β-MnO_2, δ-MnO_2, λ-MnO_2, Mn_2O_3, Mn_3O_4, amorphous manganese oxides, octahedral molecular sieves, and octahedral layered manganese oxides have been studied for water oxidation (10-14). Nanosized manganese oxide supported on mesoporous silica (KIT-6) has been reported

(15). Water oxidation are evaluated using water oxidant such as cerium ammonium nitrate (CAN), photochemical water oxidation using photosensitizer such as $Ru(bpy)_3^{2+}$, or photoelectrochemically.

We report the synthesis of birnessite like poorly ordered layered manganese oxides supported on zeolite Y microstructure and evalutate its photocatalytic water oxidation activity. We are using zeolite Y as the support for manganese oxides catalyst. Zeolites are hydrated microporous aluminosilicate minerals with the pores and cavities in molecular dimensions as shown in Figure 3. It has the framework consisting of T-O-T (T=Si/Al) connecting TO_4 tetrahedr a (16). They possess large surface area and tunable surface properties. Zeolite Y has Si/Al ratio of 2.5 with sodium ions as a counterbalance charge. It has a pore size of 7 A^o and supercage of 13 A^o (16). The ion-exchanging properties, high surface area, and high thermal stability of zeolite Y have broadened the range of its applications. The synthesis of nanoscale manganese oxides within faujasite zeolite has already been reported in the literature and oxygen evolution kinetics was measured using CAN (17). Our group reported the anchoring of cobalt hydroxide on the surface of zeolite Y resulting better stability of catalyst through immobilization and better dispersion on the zeolite surface (18). We adopt similar a novel synthetic route to synthesize manganese oxides on the zeolite surface. Mn^{2+} ions are ion-exchanged into zeolite, and then treated with $KMnO_4$. K^+ ion-exchanges out Mn^{2+} from zeolite, and reacts with MnO_4^- to form manganese oxides on the surface of zeolite. We hypothesize that zeolite Y can enhance the catalytic activity of manganese oxides by uniformly dispersing manganese oxides on its surface, immobilizing and stabilizing them, controlling their size and morphology, and exposing more active Mn sites to photosensitizers for efficient photocatalytic water oxidation.

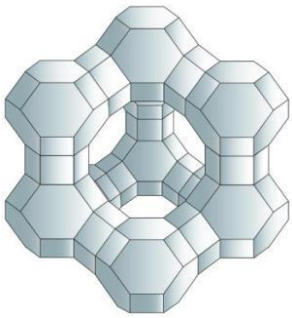

Figure 3: Zeolite Y microstructure

Experimental Section:

Synthesis of zeolite supported manganese oxides: Micron-sized zeolite Y (Si/Al= 2.55) was purchased from Zeolyst International. A typical experiment is defined. In 200 mL of 0.04 M manganese (II) acetate tetrahydrate (Sigma Aldrich) 2.0 g of zeolite Y. The ion-exchange at room temperature (RT) was carried out for 24 h. The solution was filtered and washed and dried overnight at RT, and further treated with 100 mL of 0.01 M $KMnO_4$ and stirred for 2h at RT followed by filtration, washing, and drying. These samples are called MnOx-Y*. Further treatment included stirring with 50 mL of 3.0 M KCl for 2h at RT followed by filtration, washing, and drying at RT. The resulting materials are named MnOx-Y.

Synthesis of bulk manganese oxides (MnOx): In a 100 mL, 0.04 M manganese (II) acetate and 0.01 M $KMnO_4$ were stirred for 2 hours at RT. The solution was filtered and washed and dried overnight at RT. The samples were further treated with 50 mL of 3.0M KCl for 2h at RT followed by filtration, washing, and drying at RT.

Characterization: X-ray diffraction patterns were obtained using a Rigaku X-ray diffractometer with Cu Kα radiation with 0.5 divergence, 0.02 step size and 0.5s dwell time. Raman spectroscopy was done with a Renishaw-Smith Detection IR-Raman Microprobe, model- inVia. A 633-laser line was used for the acquisition of the spectra. A spinning cell was used in order to preserve the sample integrity. XPS sepctra was obtained using Kratos Axis Ultra X-ray photoelectron

spectrometer with Al K∞ source (12 kV, 6 mA). The region scans were acquired using 20 eV pass energy and the survey scan was obtained using 80 eV. All peaks were calibrated with respect to C 1s peak position at 285.0 eV. The morphology of the samples was characterized by FEI Helios Nanolab 600 dual beam focused ion beam/scanning electron microscope. High-resolution transmission electron microscopy of the samples was obtained using Titan3 80-200 probe-corrected monochromated at voltage of about 140 kV.

Elemental Analysis: For elemental analysis of the catalyst, cold digestion method was adopted (19). In a Teflon bottle, 30 mL of mixed HF, HCl, and HNO_3 (1:1:1 ratio) was prepared. The catalyst (30-50 mg) was added to the acid solution. After dissolution of the catalyst, 75 mL of 0.86 M boric acid was added to neutralize HF. DI water was added to the solution so that the total solution weighs 100g. Manganese loading in the zeolite was determined using atomic absorption spectroscopy (AAS) using a Shimadzu AA-7000 Atomic Absorption Spectrophotometer.

Photochemical water oxidation: In a glass reactor, sodium persulfate (0.02 M) (Sigma Aldrich), sodium sulfate (0.1 M) (Fischer Scientific), tris(2,2'-bipyridyl) ruthenium chloride (6.7 mg) (Sigma Aldrich), and 60 mg of powder catalyst was added to 80 mL borate buffer (pH 8.5). The solution inside the reactor was sealed and purged with N_2 gas for 10 min while stirring. After N_2 purging, the reactor was illuminated with visible light using a Hg lamp equipped with a 420 nm cut-off filter and 360 mW/cm^2 intensity. For the measurement of dissolved oxygen evolution, a YSI instrument fiber optic dissolved oxygen (YSI ProODO) sensor was used. The electrode was calibrated by 2-point calibration method (zero for nitrogen saturated water and air-saturated water).

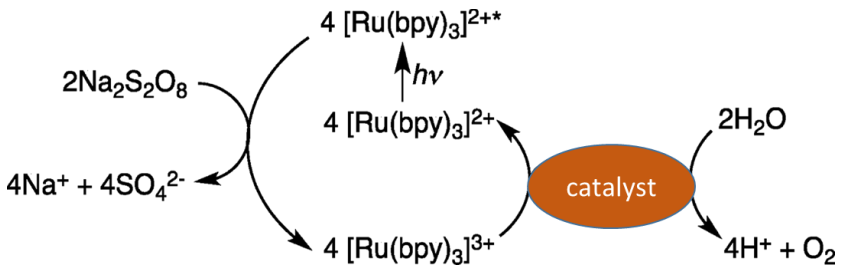

Scheme 1: Schematic diagram of photochemical water oxidation using $Ru(bpy)_3^{2+}$- $S_2O_8^{2-}$ photochemical system

Results:

Synthesis of zeolite supported manganese oxides: Scheme 2 shows the synthesis procedure outline and scheme 3 demonstrates schematic diagram of synthesis procedure. Mn^{2+} are ion-exchanged into zeolite Y. The material is treated with $KMnO_4$. During this treatment, K^+ ion-exchange out Mn^{2+} from the zeolite. Mn^{2+} reacts with the solution based MnO_4^- to form manganese oxides on the surface of zeolite (MnOx-Y*). MnOx-Y* sample is treated with high concentration of K^+ which ion-exchanges into both zeolite and manganese oxides, and is called MnOx-Y.

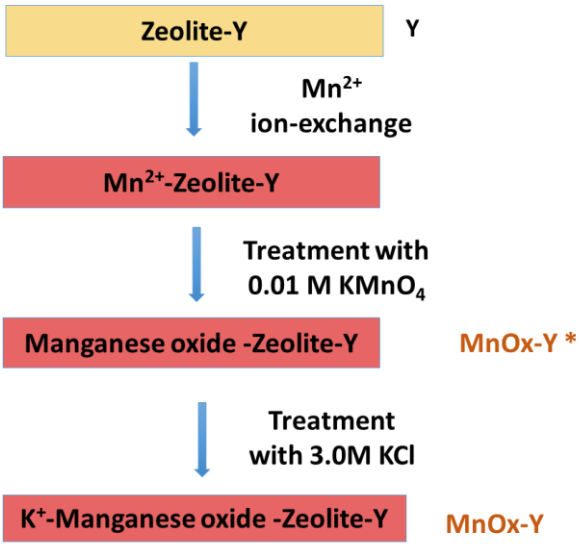

Scheme 2: Schematic outline of the synthesis procedure for MnOx-Y* and MnOx-Y

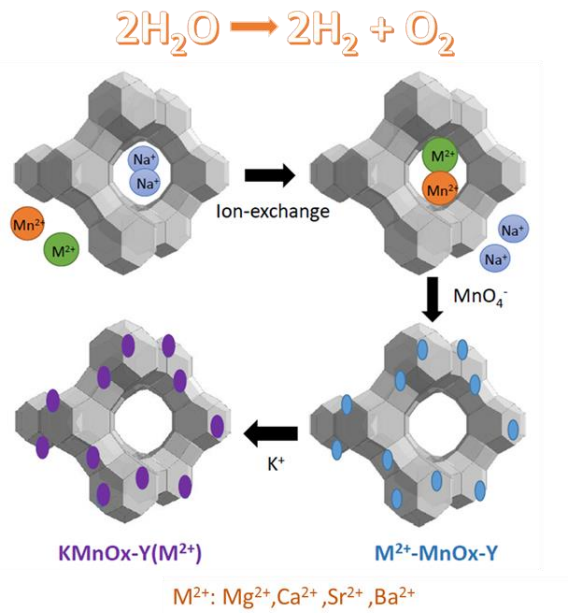

Scheme 3: Schematic diagram of the synthesis procedure for MnOx-Y* and MnOx-Y

The amount of Mn loading on zeolite Y was determined using cold digestion method, and the elemental analysis data shows that Mn wt% of MnOx-Y* is 27.7%, that of MnOx-Y is 19.2%, and that of MnOx is 49.4%.

Powder X-ray diffraction (XRD): The XRD diffraction patterns of MnOx-Y* and MnOx-Y are shown in Figure 4(a). MnOx-Y* are amorphous in nature, as no additional peaks besides zeolite Y peaks were observed. After K^+ exchange, the crystalline peaks were observed in MnOx-Y. The broad peaks at $2\theta \sim 12.5^o$, 24^o, 35.6^o, and 36.2^o were observed, which matches to the poorly ordered birnessite like layered manganese oxides (20). Since the broad peaks have weak intensities, and this signify that materials are poorly crystalline.

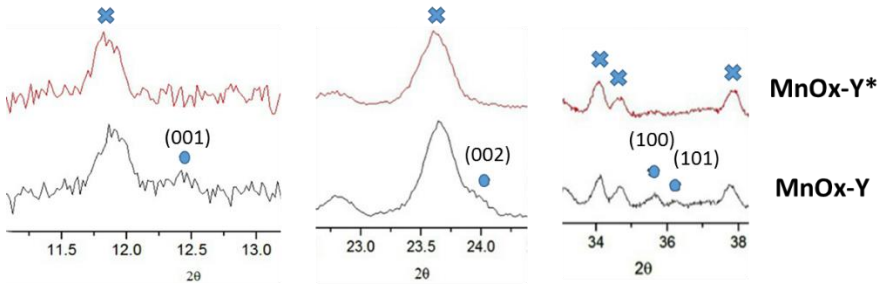

Figure 4(a): Power X-ray diffraction pattern of MnOx-Y* and MnOx-Y ranging from 2θ = 11-14º, 22-25º, and 34-37º. "x" denotes zeolite peaks and "o" denotes manganese oxides peaks

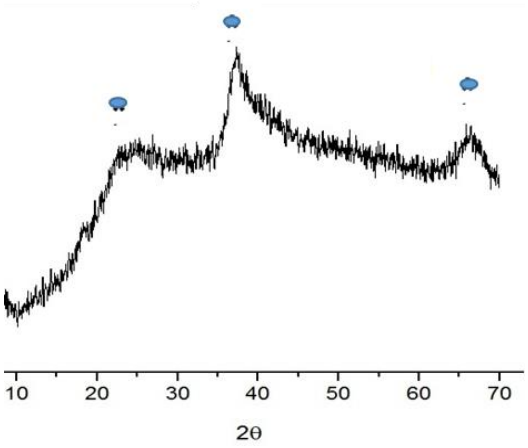

Figure 4(b): Power X-ray diffraction pattern of MnOx

Bulk manganese oxides (MnOx) have the broad crystalline peaks at 2θ ~ 24º, 38.2º, and 66º as shown in Figure 4 (b). These materials are mostly amorphous.

Raman Spectroscopy: Raman spectra of MnOx-Y* and MnOx-Y are shown in Figure 5(a) and that of MnOx is shown in Figure 5(b). Raman frequency bands are observed at ~500, 572, and 650 cm^{-1}, with the latter bands being intense as seen in all samples. Raman active modes at 500-515, 575-585, and 625-650 cm^{-1} are assigned to birnessites (21). The peak ~500 cm^{-1} overlaps with T-O-T stretching mode of zeolite Y (22). In bulk MnOx, the peak 500 cm^{-1} is relatively weak compared to MnOx-Y* and MnOx-Y because of the absence of zeolite support. The peak at ~572 cm^{-1} is attributed to Mn-O lattice vibration along the chains of MnO_6 octahedra, and the peak at ~650 cm^{-1} is attributed to symmetric stretching of Mn-O bond perpendicular to the chains of MnO_6 octahedra (11,20).

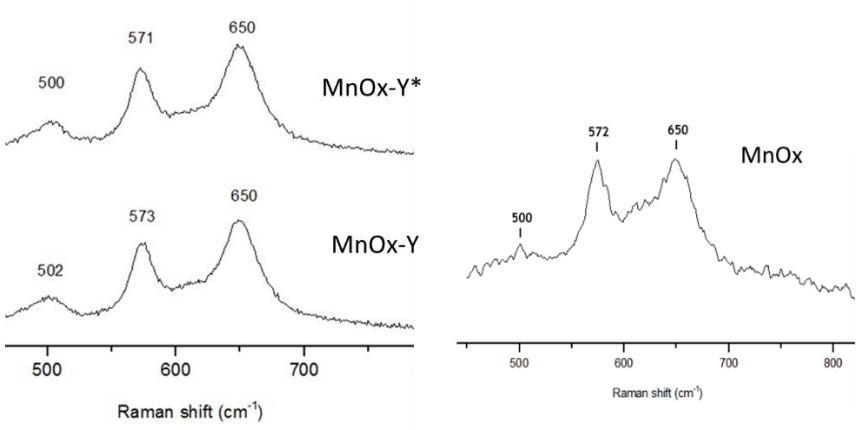

(a) (b)

Figure 5: Raman spectra of MnOx-Y* and MnOx-Y (a) and MnOx (b)

X-ray photoelectron spectroscopy (XPS): Figure 6 shows that the XPS spectra in Mn $2p_{1/2}$ and Mn $2p_{3/2}$ region for (a) MnOx-Y* (b) MnOx-Y and (c) MnOx. The curve deconvolution of Mn $2p_{3/2}$ region showed that MnOx-Y* has peaks at 642.5 and 644.3 eV, with the former being intense. For MnOx-Y, only peak at 642.5 eV was present. For MnOx, peaks at 641.3, 642.5, and 644.0 eV were present. It has been reported that Mn (III) redox state has peak at binding energy 642 eV and Mn (II)/Mn(IV) has peaks at 644 eV (23).

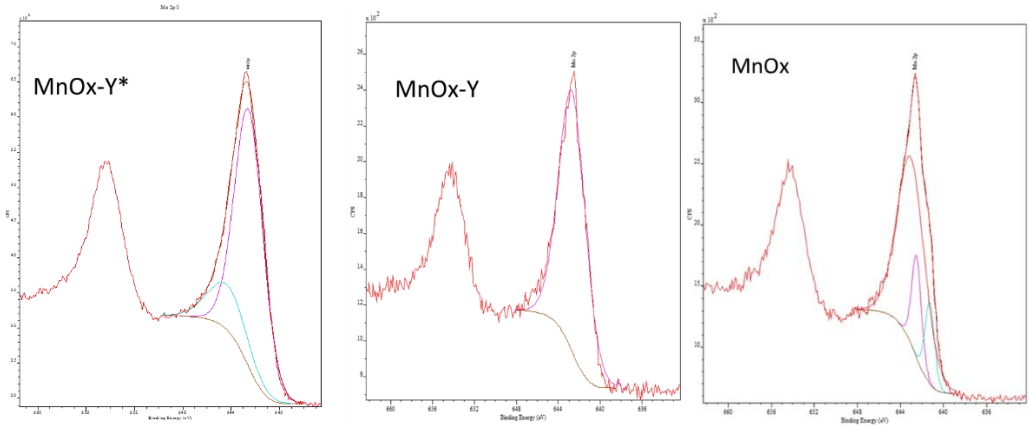

(a) (b) (c)

Figure 6: XPS spectra of Mn 2p region of (a) MnOx-Y* (b) MnOx-Y and (c) MnOx

Morphology: SEM micrographs of (a) bulk MnOx and (b) MnOx-Y are shown in Figure 7. Bulk MnOx looks micron-sized cluster. MnOx-Y* and MnOx-Y look similar in morphology (not mentioned in the paper). The zeolite is micron-sized and nanoclusters of manganese oxides are deposited on the surface of zeolite as shown in Figure 7(b). Nanosized birnessite like manganese oxides are anchored and widely dispersed on the zeolite surface. Figure 7(c) shows that lower loading of manganese oxides supported on the zeolite surface (MnOx-Y(B)).

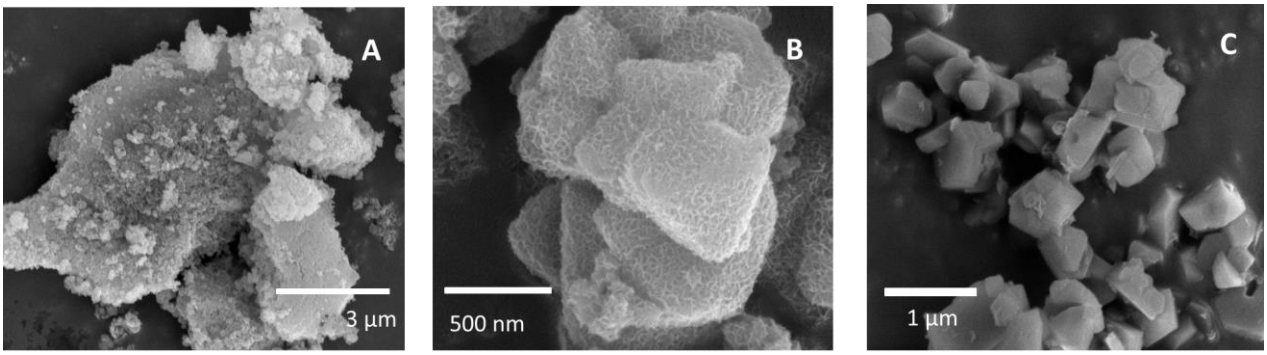

Figure 7: SEM micrographs of (a) bulk MnOx (b) MnOx-Y (19.2% Mn wt) and (c) MnOx-Y (B) (2.91% Mn wt)

Photocatalytic activity: Chemical water oxidation using CAN (0.1M) was used for evaluation of water oxidation activity using MnOx-Y. Reusability test was carried out using CAN. The rate of oxygen evolution per mole of Mn per sec (turnover frequency: TOF) was measured for three runs. The first run was 0.96, the second run was 0.24, and the third run was 0.16 $mmol_{O2}mol^{-1}{}_{Mn}s^{-1}$. XRD of MnOx-Y sample after first run was carried out (Figure S1), which showed that zeolite Y structure is completely destroyed after treatment with CAN due to low pH condition. This was not determined in the earlier paper that studied manganese oxides within faujasite zeolite for water oxidation using CAN (17). This shows that zeolite support is important for robustness and stability of manganese oxides.

Photochemical water oxidation activities of the samples were determined by using photosensitizer $Ru(bpy)_3^{2+}$ and sacrificial electron acceptor ($Na_2S_2O_8$) in borate buffer pH 8.5. The dissolved oxygen kinetics was determined by YSI optical probe. The TOF was determined for the first 100 sec. The TOF of MnOx-Y was 0.44 $mmol_{O2}mol^{-1}_{Mn}s^{-1}$ and that of MnOx was 0.048 $mmol_{O2}mol^{-1}_{Mn}s^{-1}$. The catalytic activity of MnOx-Y was better than MnOx as shown in Figure 8. Different manganese loading of MnOx-Y were synthesized. MnOx-Y(A), MnOx-Y(B), and MnOx-Y(C) have manganese weight percentage of 0.33%, 2.91%, and 19.2% respectively. The TOF of MnOx-Y(A), MnOx-Y(B), and MnOx-Y(C) were 9.05, 1.31, and 0.44 $mmol_{O2}mol^{-1}_{Mn}s^{-1}$ respectively. With the decrease in manganese loading in zeolite Y, the catalytic rate was increased as shown in Figure 9.

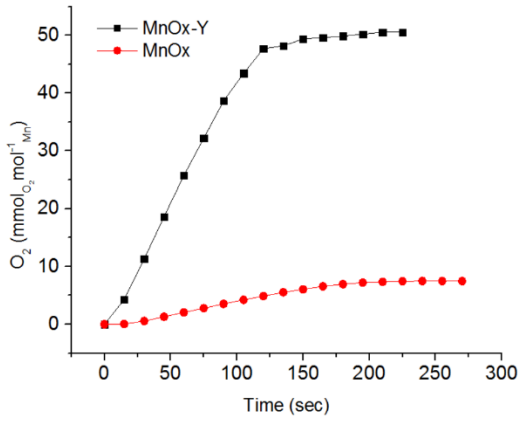

Figure 8: Visible light-induced dissolved oxygen measurement of MnOx and MnOx-Y

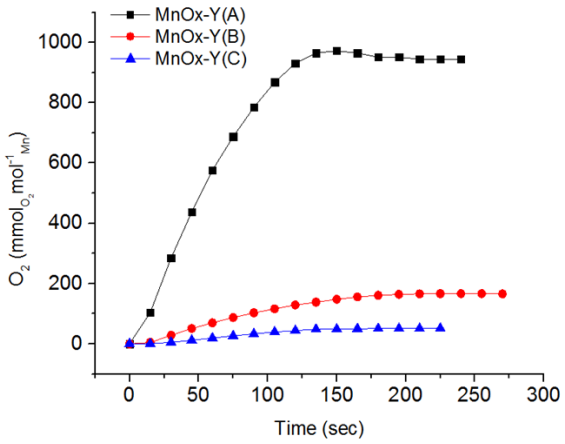

Figure 9: Visible light-induced dissolved oxygen measurement of zeolite supported manganese oxides with different loading of Mn:MnOx-Y(A) (0.33% Mn wt), MnOx-Y(B) (2.91% Mn wt) and MnOx-Y(C) (19.2% Mn wt)

Dissolved oxygen evolution kinetics of MnOx-Y* and MnOx-Y were compared. The TOF of MnOx-Y* was 0.06 $mmol_{O2}mol^{-1}{}_{Mn}s^{-1}$ and that of MnOx-Y was 0.44 $mmol_{O2}mol^{-1}{}_{Mn}s^{-1}$. The catalytic activity of the MnOx-Y* was lower compared tot hat of MnOx-Y. Treatment of MnOx-Y* with the high concentration of K^+ ions enhanced its catalytic activity as shown in Figure 10.

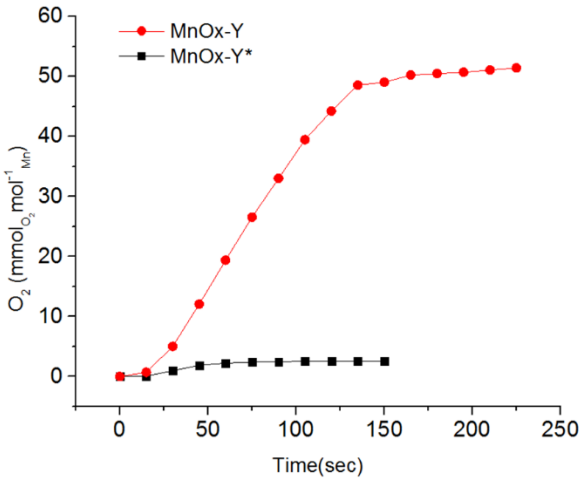

Figure 10: Visible light –induced dissolved oxygen measurement of MnOx-Y* and MnOx-Y

The active catalyst MnOx-Y was tested for reusability. The catalyst was tested twice and showed comparable performance with rates of 0.49 $mmol_{O2}mol^{-1}{}_{Mn}s^{-1}$ as shown in Figure 11. There was little oxygen evolution without catalyst in $Ru(bpy)_3^{2+}$- $S_2O_8^{2-}$ system.

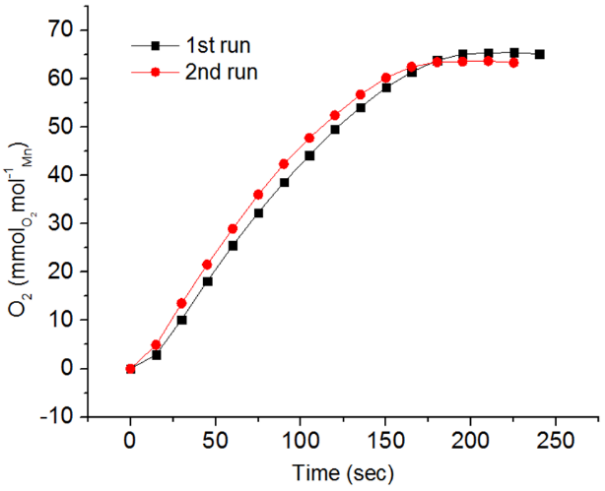

Figure 11: Reusability test of MnOx-Y in visible induced photochemical water oxidation

Discussion:

A novel non-impregnation route for the synthesis of zeolite supported manganese oxides is reported in this paper. Mn^{2+} are ion-exchanged into zeolite Y, and with the treatment of $KMnO_4$, K^+ ion-exchange out Mn^{2+} from the zeolite and Mn^{2+} reacts with the solution based MnO_4^- to form manganese oxides on the solution interface of zeolite. Thus formed MnOx-Y* are amorphous, but after treatment with high concentration of K^+ the sample MnOx-Y become poorly crystalline birnessite like layered manganese oxides.

In order to study the role of zeolite support on photocatalytic activity, bulk MnOx was prepared and its catalytic activity was compared to MnOx-Y. The photocatalytic activity of MnOx-Y was significantly higher compared to bulk MnOx as shown in Figure 8. Zeolite support plays an important role in enhancing the catalytic activity of manganese oxides. Zeolite support controls the size as well as morphology of manganese oxides, such that nano-sized manganese oxides are formed on the surface of zeolite as seen in SEM micrographs as shown in Figure 7 (b) and 7(c). Nano-sized manganese oxides has high surface-to-volume ratio compared to bulk MnOx, which can be attributed to one of the reason for increased catalytic activity of MnOx-Y. Manganese

oxides are also widely dispersed on the zeolite surface including stability as well as immobilization, leading to more exposure of Mn active sites to photosensitizers for proficient electron transfer between them for efficient water oxidation.

The loading of manganese oxides can be controlled by the amount of manganese precursors used in the first step while ion-exchanging into zeolite microstructure. Zeolite structure plays an important role in controlling the loading of manganese oxides as well. As shown in Figure 7(c), the amount of manganese oxides on zeolite surface has decreased by using the low concentration of manganese precursors. The catalytic activity of zeolite supported manganese oxides with different Mn content are shown in Figure 9, and the trend was MnOx-Y(A)> MnOx-Y(B)>MnOx-Y(C). Here the MnOx-Y(C) is referred as MnOx-Y. The lower loading of manganese oxides on zeolite, the better the performance of water oxidation. This observation is related to the effect of lower loading of manganese where the catalytic rate is normalized to Mn content. Overall, this shows that zeolite microstructure is important for optimizing the loading of manganese oxides on its surface.

The broad and weak intensities of basal reflections (001) and (002) signify that manganese oxides on the surface of zeolite (MnOx-Y) are poorly ordered and randomly stacked birnessites after K^+ treatment (24). There is an increase in random ordering of manganese oxides into crystalline phases which is helping to stabilize the layered structure of manganese oxides (25). Birnessite with random ordering and poorly crystalline nature are found to be active in catalytic water oxidation (25, 26). XPS indicate that MnOx-Y sample has predominant Mn(III) oxidation state. In bulk MnOx, there is a high content of Mn(II)/Mn(IV) oxidation state. In case of MnOx-Y*, there is high ratio of Mn(III) to Mn(II)/Mn(IV). There is an increase in content of Mn(III) after treatment with K^+ ions i.e. from MnOx-Y* to MnOx-Y. Increased Mn (III) can lead to disordering

due to lattice strain induced by Jahn-Teller distortion (20). It has been reported that Mn(III) lead to more structural flexibility, formation of Mn-O-Mn motifs for O-O bond groups, mono μ-oxo and mono μ-hydroxo groups which are linked to high oxidation activity of manganese oxides (27). Raman spectra of MnOx-Y shows that there is decrease in intensity of 572 cm^{-1} compared to 650 cm^{-1} band, which suggests that presence of local disorder in the structure of birnessite (21). This can be related to the presence of unsaturated oxygens due to disruption of Mn-O bonding in the sheets, which can participate in proton couple electron transfer for water oxidation (11). This introduction of K^+ ions into MnOx-Y* has really improved the crystallinity of manganese oxides into poorly ordered birnessite, and thus related to the increased catalytic activity of manganese oxides as shown in Figure 10. These counterbalancing cations do not have any catalytic role, but to be involved in the stabilization of layered structure of manganese oxides. MnOx-Y are stable and robust from reusability test in Figure 11. That suggests that zeolite supported manganese oxides can be reused multiple times, and still retain its structure-function property.

Comparison with Literature:

The photochemical water oxidation catalytic rates of different manganese oxides reported in the literature are listed in Table 1. They are compared to our catalyst, as they all are studied in $Ru(bpy)_3^{2+}$ photochemical system. Our catalyst has a wide range of TOF depending on the Mn content on the zeolite surface.

Catalysts	TOF ($mmol_{O2}mol^{-1}_{Mn}$ s^{-1})	Ref
MnOx-Y(K^+)	0.44-9.05	This work
Amorphous manganese oxide	0.06	11
α – MnO_2 nanowires	0.059	10
Bulk α – MnO_2	0.01	10
β - MnO_2 nanowires	0.02	10
Nano-sized λ - MnO_2	0.03	13
Mn_2O_3	1.90	28
MnOx	0.84	26

Table 1: Literature report of photochemical water oxidation activity of reported manganese oxides

Conclusion:

A successful deposition of nano-sized manganese oxides on the surface of zeolite following a novel synthetic route is demonstrated in this paper. Zeolite supported manganese oxides perform better catalytic water oxidation compared to bulk manganese oxides. Zeolite support helps to widely disperse manganese oxides on its surface, control its size and morphology, and exposes more manganese to photosensitizers for efficient water oxidation. K^+ ions improve the catalytic activity of manganese oxides by introducing more ordering, stability, and crystallinity to layered structure of manganese oxides. Zeolite supported manganese oxides are stable as well as robust. In future, we will be focusing on structure-function role of redox inert and redox active cations on manganese oxides synthesized on zeolite surface to improve both rate and yield of oxygen evolution.

References:

1. Lewis, N.S. and D. G. Nocera. “Powering the planet: Chemical challenges in solar energy utilization.” Proc. Natl. Acad. Sci. U.S.A. 103 (2006): 15729-15735
2. Dlugokencky, E. and Tans, “Trends in Atmospheric Carbon Dioxide.” P. National Oceanic and Atomospheric Administration/ Earth System Research Laboratory (www.esrl.noaa.gov/gmd/ccgg/trends/). 21 March, 2016.
3. Mulder, Grietus, Jens Hetland, and Guido Lenaers. “Towards a sustainable hydrogen economy: Hydrogen Pathways and infrastructure.” International Journal of Hydrogen Energy 32 (2007): 1324-1331
4. Krol, Roel van de, Yongqi Liang, and Joop Schoonman. “Solar hydrogen production with nanostructured metal oxides.” Journals of Materials Chemistry 18 (2008): 2311-2320
5. Hara, Michikazu, Chad C. Waraksa, John T. Lean, Bradley A. Lewis, and Thomas E. Mallouk. “Photocatalytic Water Oxidation in a Buffered Tris (2,2’-bipyridyl)ruthenium Complex-Colloidal IrO_2 System.” J. Phys. Chem. A 104 (2000): 5275-5280
6. Das, Samar K. and Prabir K. Dutta. “Synthesis and characterization of a ruthenium oxide-zeolite Y catalyst for photochemical oxidation of water to dioxygen.” Microporous and Mesoporous Materials 22 (1998): 475-483
7. Yamada, Yusuke, Kentaro Yano, Dachao Hong, and Shunichi Fukuzumi. “$LaCoO_3$ acting as an efficient and robust catalyst for photocatalytic water oxidation with persulfate” Phys. Chem. Chem. Phys 14 (2012):5753-5760
8. Hong, Dachao, Yusuke Yamanda, Takaharu Nagatomi, Yoshizo Takai, and Shunichi Fukuzumi. “Catalysis of Nickel Ferrite for Photocatalytic Water Oxidation Using $[Ru(bpy)_3]^{2+}$ and $S_2O_8^{2-}$.” J. Am. Chem. Soc. 134 (2012): 19572-19575

9. Elizarova, G. L., G. M. Zhidomirov, and V. N. Parmon. “Hydroxides of transition metals as artificial catalysts for oxidation of water to disoxygen.” Catalysis Today 58 (2000): 71-88
10. Boppana, V. B. R. and Frei Jiao. “Nanostructured MnO_2: an efficient and robust water oxidizing catalyst.” Chem. Commun. 47 (2011):8973-8975
11. Iyer, Aparna, Joselyn Del-Pilar, Cecil K. King’ondu, Edward Kissel, Hector F. Garces, Hui Huang, Abdelhamid M. El-Sawy, Prabir K. Dutta, and Steven L. Suib. “Water Oxidation Catalysis using Amorphous Manganese Oxides, Octahedral Molecular Sieves (OMS-2), and Octahedral Layered (OL-1) Manganese Oxide Structures.” J. Phys. Chem. C 116 (2012): 6474-6483
12. Takashima, Toshihiro, Kazuhito Hashimoto, and Ryuhei Nakamura. “Mechanisms of pH-Dependent Activity for Water Oxidation to Molecular Oxygen by MnO_2 Electrocatalysts.” J. Am. Chem. Soc. 134 (2012): 1519-1527
13. Robinson, David M., Yonk Bok Go, Michelle Mui, Graeme Gardner, Zhijuan Zhang, Daniel Mastrogiovanni, Eric Garfunkel, Jing Li, Martha Greenblatt, and G. Charles Bismukes. “Photochemical Water Oxidation by Crystalline Polymorphs of Manganese Oxides: Structural Requirements for Catalysis.” J. Am. Chem. Soc. 135 (2013): 3494-3501
14. Zaharieva, Ivelina, Petko Chernev, Marcel Risch, Katharina Klingan, Mike Kohlhoff, Anna Fischer, and Holger Dau. “Electrosynthesis, functional, and structural characterization of a water-oxidizing manganese oxides.” Energy Environ. Sci. 5 (2012): 7081

15. Jiao, Feng, and Heinz Frei. “Nanostructured manganese oxide clusters supported on mesoporous silica as efficient oxygen-evolving catalysts.” Chem. Commun. 46 (2010): 2920-2922
16. S. M. Auerbach, K. A. Carrado, and Prabir K. Dutta. Handbook of Zeolite Science and Technology. New York : 2003. Print.
17. Najafpour, Mohammad Mahdi, Babak Pashaei. “Nanoscale manganese oxide within Faujasite zeolite as an efficient and biomimetic water oxidizing catalyst.” Dalton Trans. 41 (2012): 10156
18. Del Pilar-Albaladejo, Joselyn and Prabir K. Dutta. “Topotactic Transformation of Zeolite Supported Cobalt (II) Hydroxide to Oxide and Comparison of Photocatalytic Oxygen Evolution.” ACS Catal. 4 (2014): 9-15
19. Peru, D. A. and R. J. Collins. “Comparison of cold digestion methods for elemental analysis of a Y-type zeolite by inductively coupled plasma (ICP) spectrometry.” Fresenius J Anal Chem 346 (1993): 909-913
20. Luo, Jian, Qiuhua Zhang, and Steven L. Suib. “Mechanistic and Kinetic Studies of Crystallization of Birnessite.” Inorg. Chem. 39 (2000): 741-747
21. Julien, C,, M. Massot, R. Baddour-Hadjean, S. Franger, S. Bach., and J. P. Pereira-Ramos. “Raman spectra of birnessite manganese dioxides.” Solid State Ionics 159 (2003): 345-356
22. Dutta, Prabir K., K. Mohana Rao, and Jong Yul Park. “Correlation of Raman Spectra of Zeolites with Framework Architecture.” J. Phys. Chem. 95 (1991): 6654-6656
23. Oku, Masaoki and Kichinoskuke Hirokawa. “X-ray Photoelectron Spectroscopy of Manganese-Oxygen Systems.” Journal of Electron Spectroscopy and Related Phenomena 7(1975): 465-473

24. Villalobos, Mario, Brandy Toner, John Bargar, and Garrison Sposito. “Characterization of the manganes oxide produced by *Pseudomonas putida* Strain MnB1.’ Geochimica et Cosmochimica Acta 67 (2003): 2649-2662
25. Boppana, V. B. R. , Seif Yusuf, Gregory S. Hutchings, and Feng Jiao. “Nanostructured Alkaline-Cation-Containing δ- MnO_2 for Photocatalytic Water Oxidation.” Adv. Func. Mater. 23 (2013): 878-884
26. Deibert, Benjamin J., Jingming Zhang, Paul F. Smith, Karena W. Chapman, Sylvie Rangan, Debasis Banerjee, Kui Tan, Hao Wang, Nicholas Pasquale, Feng Chen, Ki-Bum Lee, G. Charles Dismukes, Yves J. Chabal, and Jing Li. “Surface and Structural Investigation of a MnOx Birnessite-Type Water Oxidation Catalyst Formed under Photocatalytic Conditions.” Chem. Eur. J. 21 (2015): 14218-14228
27. Zaharieva, Ivelina, M. Mahdi Najafpour, Mathias Wiechen, Michael Haumann, Philipp Kurz, and Holger Dau. “Synthetic manganese-calcium oxides mimic the water-oxidizing complex of photosynthesis functionally and structurally.” Energy Environ. Sci. 4(2011): 2400
28. Menezes, Prashanth W.; Arindam Indra, Patrick Littlewood, Michael Schwarze, Caren Gobel, Reinhard Schomacker, and Matthias Driess. “Nanostructured Manganese Oxides as Highly Active Water Oxidation Catalysts: A Boost from Manganese Precursor Chemistry.” ChemSusChem 7 (2014): 2202-2211

Supplementary Section:

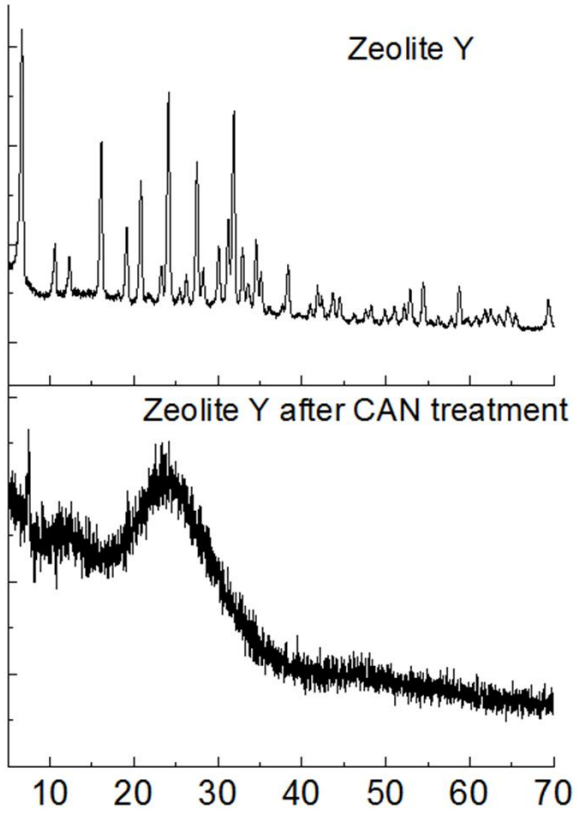

Figure S1: X-ray diffraction pattern of zeolite Y before and after treated with 0.1M CAN